Fibers and Polymers 2001, Vol.2, No.1, 163-172

Confocal Microscopy Measurement of the Fiber Orientation in Short Fiber Reinforced Plastics

Kwang Seok Lee, Seok Won Lee, Jae Ryoun Youn*, Tae Jin Kang, and Kwansoo Chung

School of Materials Science and Engineering, Seoul National University, Seoul 151-742, Korea
(Received January 30, 2001; Revised February 28, 2001; Accepted March 5, 2001)

Abstract: To determine three-dimensional fiber orientation states in injection-molded short fiber composites a CLSM (Confocal Laser Scanning Microscope) is used. Since the CLSM optically sections the composites, more than two cross-sections either on or below the surface of the composite can be obtained. Three dimensional fiber orientation states can be determined with geometric parameters of fibers on two parallel cross-sections. For experiment, carbon fiber reinforced polystyrene is examined by the CLSM. Geometric parameters of fibers are measured by image analysis. In order to compactly describe fiber orientation states, orientation tensors are used. Orientation tensors are determined at different positions of the prepared specimen. Three dimensional orientation states are obtained without the difficulty in determining the out-of-plane angles by utilizing images on two parallel planes acquired by the CLSM. Orientation states are different at different positions and show the shell-core structure along the thickness of the specimen.

Keywords: Confocal laser scanning microscopy, Injection molding, Fiber orientation, Orientation tensor, Image processing

Introduction

Short-fiber reinforced plastics (SFRP) are being widely used for technical and industrial applications due to good mechanical properties, easiness of manufacturing, and economical advantages. SFRP are usually processed by injection molding or compression molding. During molding a complex flow field is generated in a cavity. Thus the fiber orientation depends highly on the process conditions[1,2] and controls mechanical and thermal properties[3] of the final product, such as stiffness, tribology[4-6], thermal expansion, and strength. Therefore, it is important to measure the fiber orientation in real composite parts and to apply the measured fiber orientation states to characterization of local properties. Fiber orientation states can be predicted by numerical simulations and compared with the measured results.

Many different methods have been developed to determine the fiber orientation in SFRP. Among them, reflective microscopy is the most popular method for measuring orientation. It can produce images from surfaces prepared by metallographic polishing. If the cross-section of the fiber is circular, an elliptical image of fiber cross-section will appear on the intercepting plane. Then we can calculate directional angles (θ, ϕ) of fibers by measuring the principal axes of the ellipse as shown Figure 1. However, this method has some weak points. Firstly, there always exists an ambiguity of out-of-plane angle (θ) because both elliptical images of fibers oriented at angle θ and of fibers oriented at angle 180°-θ are identical. Secondly, as the cross-section of fiber is getting closer to a perfect circle, the sensitivity in the measurement of out-of-plane angle (θ) is increasing, which could lead serious errors. In order to minimize this error source resolution of the measuring instrument should be high enough. Yurgartis[7] and other researchers[8,9] sectioned specimens at an angle with respect to the melt flow direction. Although this way of sectioning can dramatically reduce the second error, the first problem still remains unsolved. Fortunately, the ambiguity can be removed by an optical-sectioning technique, where parallel planes below the surface are captured by focusing at different depth[10]. It was proposed that a confocal laser scanning microscope be used for the study of fiber-reinforced polymer composites [11]. By using the CLSM[12], more than two parallel planes below the surface can be focused so that we can remove the ambiguity in determining the out-of-plane angles.

In this work, three-dimensional fiber orientation tensors are determined without the difficulty of determining the angles. For experiments, tensile specimens are injection molded with polystyrene reinforced by 3 vol% (4.5 wt%) short carbon fibers. The specimen is examined by the CLSM at different positions and across the thickness of the specimen. By measuring the center coordinates of the fiber images appearing on the micrographs, the directional angles of fibers are determined. Finally, orientation tensors are calculated with the directional angles.

Theory

Description of fiber orientation

Assuming that the fiber is rigid and uniform in length, the orientation of fibers can be represented by using unit vectors $\boldsymbol{p}$ directed toward the end of fibers, as shown in Figure 2. The components of $\boldsymbol{p}$ are related to θ and ϕ,

$$\begin{aligned} p_1 &= \cos\theta \\ p_2 &= \sin\theta\cos\phi \\ p_3 &= \sin\theta\sin\phi \end{aligned} \tag{1}$$

*Corresponding author: jaeryoun@gong.snu.ac.kr

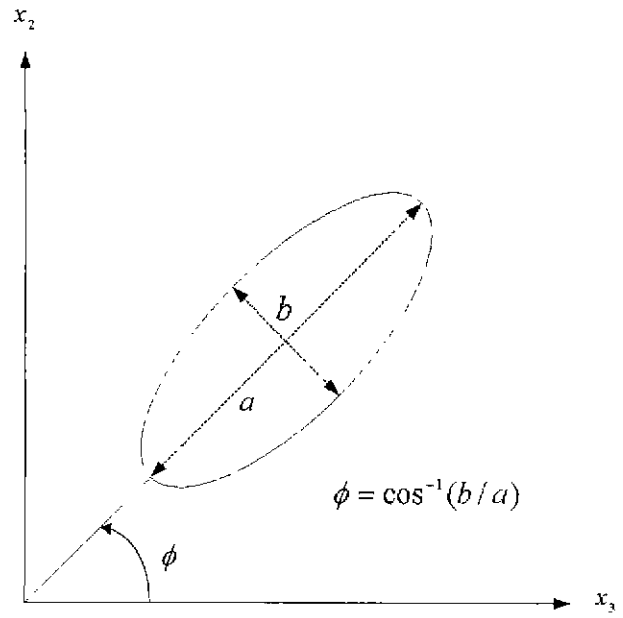

Figure 1. The elliptical image of a fiber on the sectioning plane.

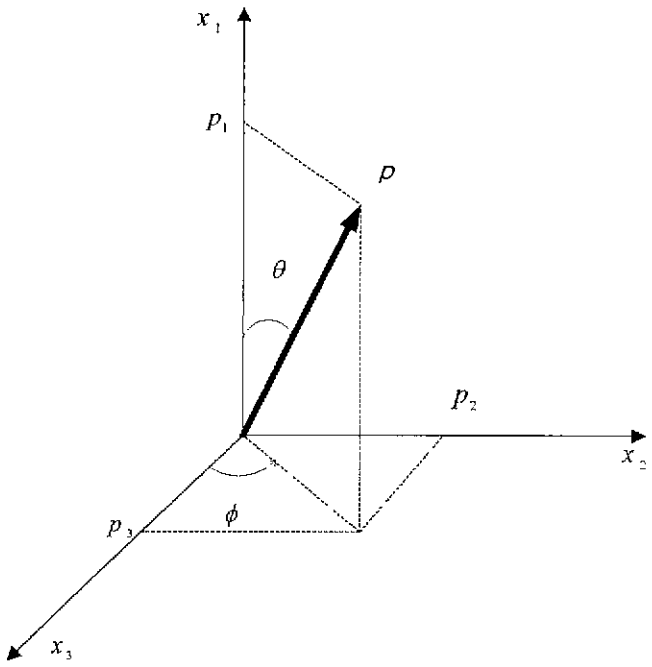

Figure 2. The coordinate system employed for representing fiber orientation.

Since two ends of the fiber are not distinguishable, the following relation holds.

$$\boldsymbol{p} = -\boldsymbol{p} \tag{2}$$

In SFRP, since the fibers are lying toward more than one direction and do not have uniform length, a description which reflects the orientation of many single fibers and variation of the length is required. One approach is to use the probability density function ψ, which gives the probability of a fiber being oriented at angles between θ_0 and $\theta_0 + d\theta$, ϕ_0 and $\phi_0 + d\phi$ having a length between L_0 and $L_0 + dL$, as follows:

$$P(\theta_0 \le \theta \le \theta_0 + d\theta,\ \phi_0 \le \phi \le \phi_0 + d\psi,\ L_0 \le L \le L_0 + dL) = \psi(\theta_0, \phi_0, L_0)\sin\theta_0 d\theta d\phi dL \tag{3}$$

Since every fiber is oriented at some angle and has some length the integration of the probability density function over all angles and every possible length must be equal to unity:

$$\int_p \int_L \psi(\boldsymbol{p}, L) dL d\boldsymbol{p} = 1 \tag{4}$$

According to the equation (2) the distribution function must be even function.

$$\psi(\boldsymbol{p}, L) = \psi(-\boldsymbol{p}, L) \tag{5}$$

Equation (5) is called the periodic condition. The distribution function $\psi(\boldsymbol{p}, L)$ is a general description of the orientation state. However, it is not practical to calculate $\psi(\boldsymbol{p}, L)$ in such an application as numerical analysis. Thus, more compact and efficient description is needed.

Another approach is to use the orientation tensors that are created by forming dyadic products of the vector $\boldsymbol{p}$ and integrating over all directions and every possible length by weighting the dyadic product with the distribution function ψ and the length L. The second orientation tensor is defined as follows:

$$a_{ij} = \frac{\int_L \int_p p_i p_j L \psi(\boldsymbol{p}, L) d\boldsymbol{p} dL}{\int_L \int_p L \psi(\boldsymbol{p}, L) d\boldsymbol{p} dL} \tag{6}$$

From these definitions, the components of orientation tensors follow the transformation rules for tensors. The orientation tensors are symmetric[13]:

$$a_{ij} = a_{ji} \tag{7}$$

From the normalization condition, trace of the second order tensor equals unity:

$$a_{ii} = 1 \tag{8}$$

In actual composites, discrete fiber samples are measured and components of the orientation tensors are calculated by summation instead of the integration as follows:

$$a_{ij} = \frac{\sum (p_i p_j) L_n F_n'}{\sum L_n F_n'} \tag{9}$$

Here, F_n' represents the weighting function for the nth fiber [14].

$$F_n' = \frac{1}{L_n \cos\theta_n} \tag{10}$$

$$F_n' = \frac{1}{d_n} \quad \text{for} \quad \theta_n = 90° \tag{11}$$

The weighting function is required because the fiber oriented normal to the sectioning plane is more likely to intercept the plane than the fiber oriented parallel to the plane. F_n also represents the projected height of the fiber onto the axis normal to the sectioning plane. In the case of fibers lying perfectly parallel to the sectioning plane, the fiber diameter can be substituted for the height of fiber. Therefore equation (9) becomes

$$a_{ij} = \frac{\sum(p_i p_j)F_n}{\sum F_n} \tag{12}$$

$$\text{where } F_n = \frac{1}{\cos\theta_n} \tag{13}$$

$$F_n = L/d \quad \text{for} \quad \theta_n = 90° \tag{14}$$

L is the length of the fiber and d is the diameter of the fiber.

Principles of confocal laser scanning microscopy

Simplified optics of the CLSM[15,16] is shown schematically in Figure 3. A laser beam from either argon or krypton laser go through a dichroic mirror (beam splitter) and microscope optics, and illuminates a sample. The reflected light and any fluorescence emission from the sample return through the microscope optics, the beam splitter, an emission filter, and a detecter pinhole (confocal aperture) before reaching a photodetector (photomultiplier, PMT). The emission filter selects either the reflected light or the longer wavelength fluorescence light. The former is referred as the reflection mode and the latter as the fluorescence mode. Mirrors scan the laser beam in both X and Y directions so that an optical XY plane should be defined. The role of the confocal aperture is removing out-of-focus light. As decreasing the size of the aperture, the regional image of the focal plane becomes thinner. A focal plane may be placed at the sample surface or within the sample by moving Z-drive on the microscope.

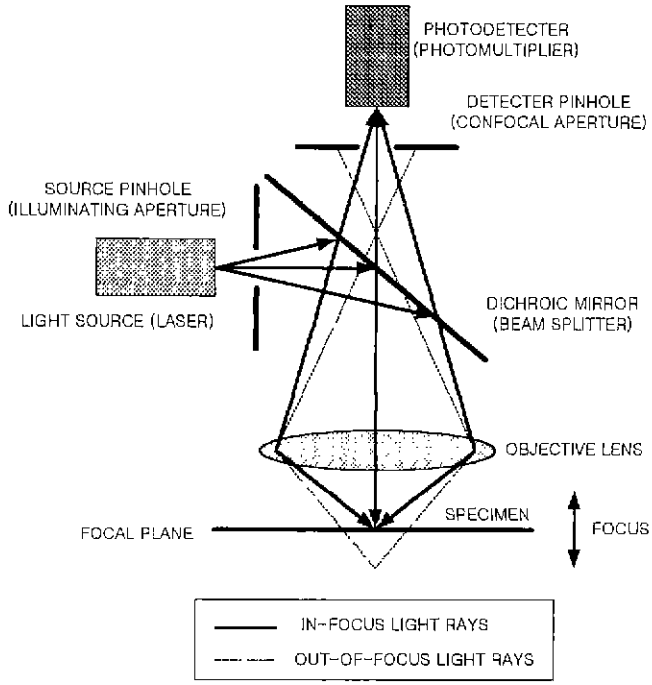

Figure 3. Simplified optics of a confocal laser scanning microscope.

In order to achieve high quality of optical sectioning, a high numerical aperture (NA) lens should be used for the microscope objective and the sample should be sufficiently transparent or at least semi-transparent.

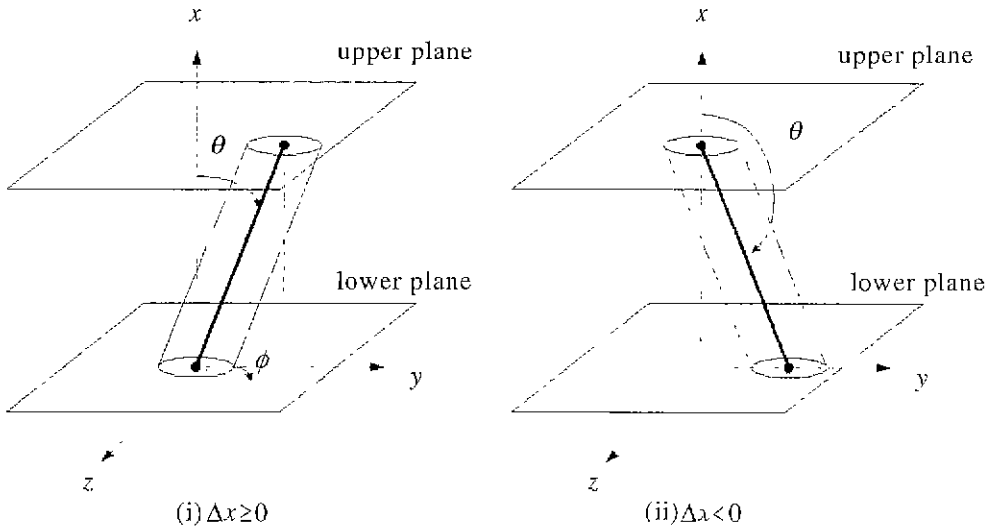

Figure 4. The coordinate system employed to define directional angles.

Calculation of orientation tensors with the CLSM

Since the CLSM is capable of optical sectioning, more than two parallel planes within the sample can be examined. Assuming that each image of a single fiber on two parallel planes is identical, the directional angles (θ, ϕ) can be determined by using center coordinates of the two image as shown in Figure 4.

$$\theta = \tan^{-1}\left(\frac{\Delta r}{\Delta z}\right), \qquad \Delta x \geq 0 \tag{15}$$

$$\theta = 180^{\circ} - \tan^{-1}\left(\frac{\Delta r}{\Delta z}\right), \qquad \Delta x = 0 \tag{16}$$

$$\phi = \tan^{-1}\left(\frac{\Delta y}{\Delta x}\right) \tag{17}$$

$$\text{where } \Delta r = \sqrt{\Delta x^2 + \Delta y^2} \tag{18}$$

Δx and Δy are the differences between the center coordinates of two images.

$$\Delta x = x_{upper} - x_{lower} \tag{19}$$

$$\Delta y = y_{upper} - y_{lower} \tag{20}$$

Δr is the distance between two center coordinates and Δz is the difference between upper and lower planes.

After determining directional angles orientation tensors can be calculated by summing the dyadic products weighted with F_n with equations (12) to (14). In the case of fibers lying almost parallel to the sectioning plane, two center coordinates of individual fibers are located far apart. In the case of fibers normal to the sectioning plane, two center coordinates of each image of the fiber are identical. In the experiment, fibers oriented between $\theta = 80^{\circ}$ and $\theta = 110^{\circ}$ are sensitive to the error mentioned above. To remove the error, the major and minor axes of fibers oriented at this range are measured and used for determination of the out-of-plane angle (θ). If the major axis is much greater than the minor axis, the out-of-plane angle (θ) is determined as shown in Figure 1.

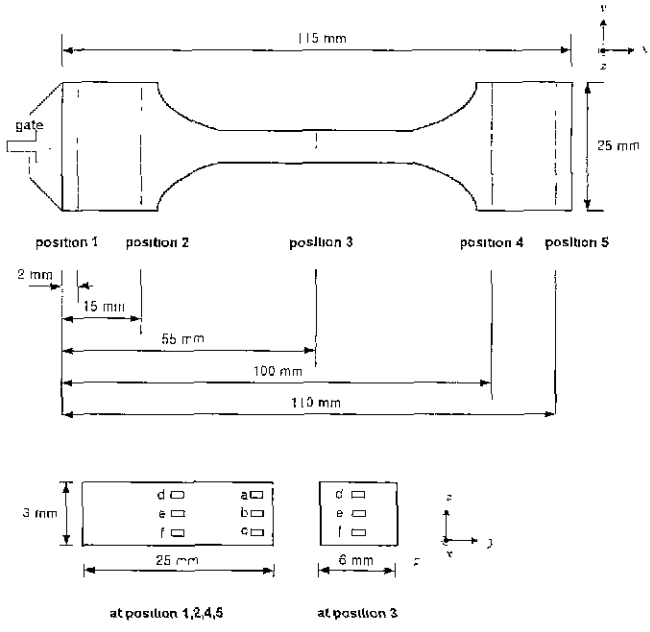

Figure 5. Dimensions of the specimen, sampling positions, and observed locations.

Experimental

Tensile specimens were injection molded in order to determine the orientation tenors at different positions. A film-gated cavity is used for molding and geometric dimensions are shown in Figure 5. Samples were prepared from the

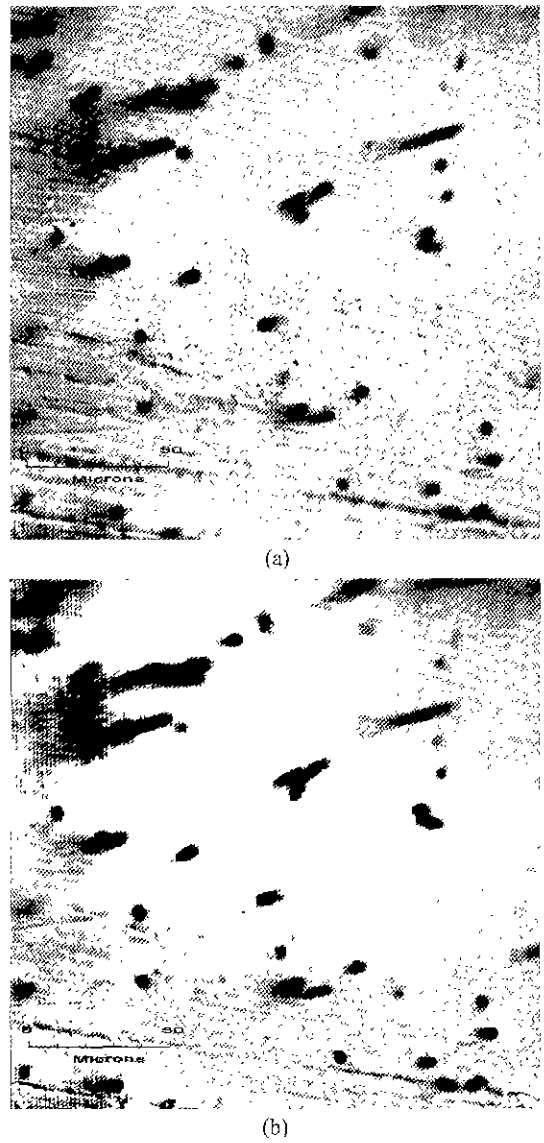

Figure 6. Typical micrographs taken by the CLSM. (a) upper sectioning plane, (b) lower sectioning plane.

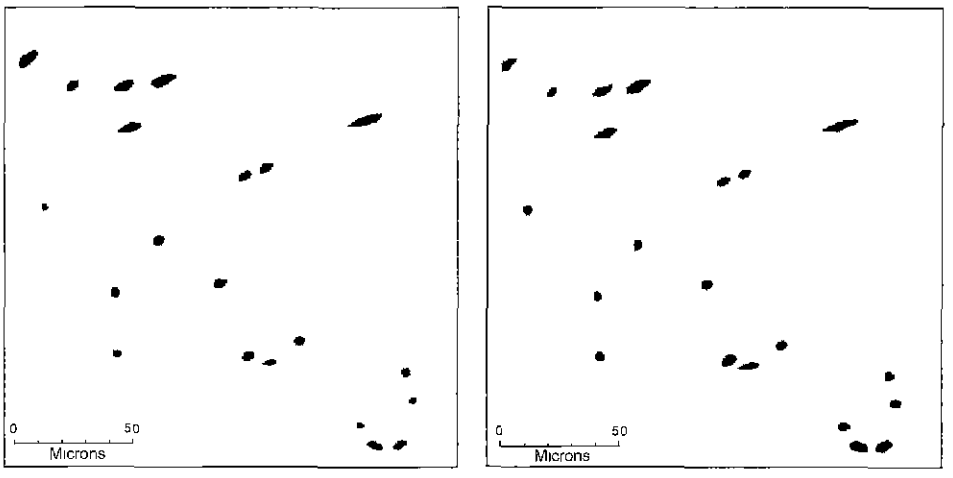

(a) (b)

Figure 7. Typical images after thresholding: (a) upper sectioning plane, (b) lower sectioning plane.

specimen at different positions. Each sample was optically sectioned by 1 μm. Geometric parameters of fiber images on the two parallel planes selected were measured by using image processing techniques. From measured data the orientation tensors were calculated by using a simple computer code.

Starting materials

6 mm long chopped carbon fibers (supplied by Taekwang Industrial Co.) and polystyrene (GPPS HF-2680, supplied by Cheil Industries) were used for injection molding. The average fiber diameter was 6.8 μm according to supplier.

The pellets of polystyrene reinforced with 3 vol% (4.5 wt%) carbon fibers were processed by the extrusion process at 200°C in a twin screw extruder (PRISM, UK) and the extrudates were cut into pellets.

Process conditions for injection molding

The specimens were molded by using an injection molding machine (Battenfeld). The injection pressure was 8 MPa, holding pressure was 7.5 MPa, barrel temperature was 200°C, mold temperature was 60°C, filling time was 1.6 sec, holding time was 5 sec, and cooling time was 25 sec.

Sample preparation and optical sectioning with the CLSM

Samples were prepared from the specimen by cutting normal to the flow direction at the five different positions (position 1~5) as shown in Figure 5 and each sample was polished by using the metallographic method[17]. Finer grades of silicon carbide papers, lubricated with water, were used successively to obtain good quality of polishing (320, 800, 1200, 2000, 4000 SiC paper grade). Final thickness of the sample was about 1 mm. Each sample was placed on the slide glass and squared paper was used to align the samples.

Six points (a to f) on each sample were observed by the CLSM. Three points (d, e, f) were observed for the sample acquired from position 3. Specific locations of the points are described in Figure 5. Images of 20 to 30 cross-sections at each point were obtained by using the optical sectioning technique and the separation of optical sectioning was 1 μm. For the optical sectioning, Bio-Rad Radian 2000MP was employed with the objective of NA 0.75 (×40 magnification) and the eyepiece of ×10 magnification, and operated on the transmission mode. Actual size of the observed domain was 187 μm × 187 μm. The original micrographs obtained by CLSM are shown in Figure 6.

Image processing and orientation tensor calculation

Two cross-sections separated by 10 μm were selected for the image processing[18-20]. The image processing was conducted by using a commercial image analysis tool (Image-Pro Plus 4.1, Media Cybernetics®). The sections were first enhanced by controlling the contrast and brightness of images and then transformed into binary images by the thresholding method in order to discard other unnecessary images such as dusts and cracks. The fiber images which are overlapped each other due to insufficient axial resolution or the fiber images intercepting the boundary of the domain were removed by manual operation. Figure 7 shows the examples of images after thresholding process.

From given fiber images of the two sections, geometric parameters, center coordinates, major axes, minor axes, and in-plane directional angles (ϕ), were measured. The two directional angles (θ, ϕ) of fibers were calculated from the difference between the center coordinates of the upper and lower planes by using equations (15) to (20). The orientation tensors are calculated by equations (12) to (14). In the experiment, 10~30 fibers were measured in each section.

Results and Discussion

Orientation states along the flow direction

Components of orientation tensors measured along at the edge (point 'a') of the specimen are shown in Figures 8. Diagonal components are shown in (a) and off-diagonal components are shown in (b) of the figure. If the off-diagonal components are zero, the diagonal components describe the orientation distribution of fibers along the x, y, and z directions. Therefore, non-zero off-diagonal components indicate that x, y, and z axes are not the principal axes[21]. The sign of a_{12} changes from positive to negative at the position 2, which means that fibers rotate to the other side in the x-y plane at the converging region. Since all components except for a_{11} are close to zero at the position 4, fibers are fully aligned to the x-direction. Figure 9 shows orientation states along the point 'c'. The non-zero values of a_{13}, which vary from –0.09 to 0.25, imply that the principal direction of orientation is tilted out of the x-y plane. Because the location of the film gate is close to the lower plane the value of a_{13} at position 1 in Figure 9 is larger than that in Figure 8. From the fact, it is obvious that the fiber orientation is strongly affected by the flow toward z-direction near the gate.

Figures 10 and 11 show the values of orientation tensor along the centerline. In Figure 10, random fiber orientation states appear at every position along the point 'e'. Since out-of-plane component (a_{13}) at the position 3 is smaller than

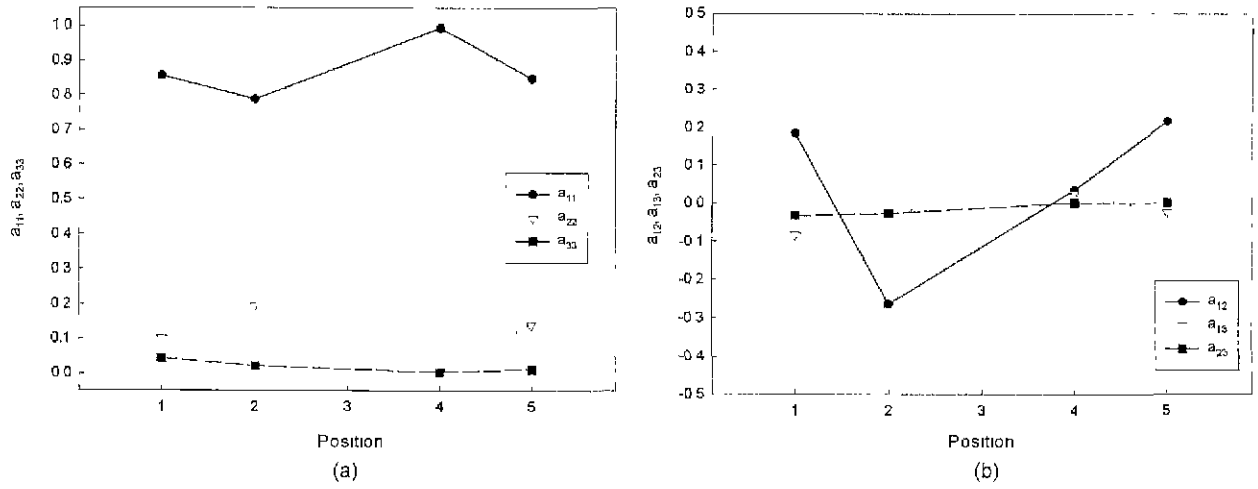

Figure 8. Components of the orientation tensor along the location **'a'** defined in Figure 5 at different positions: (a) diagonal components, (b) off-diagonal components.

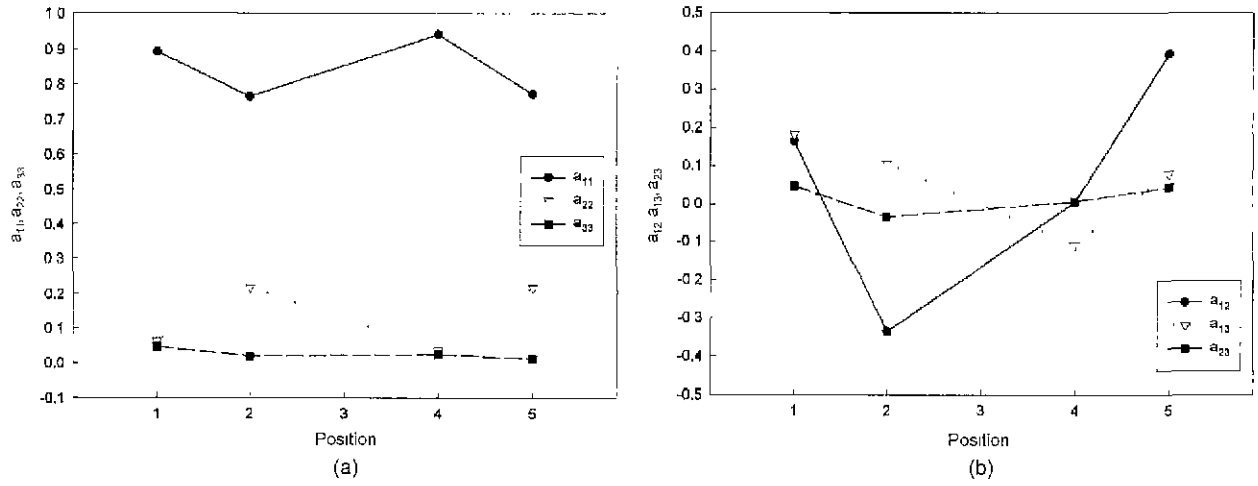

Figure 9. Components of the orientation tensor along the location **'c'** defined in Figure 5 at different positions: (a) diagonal components, (b) off-diagonal components.

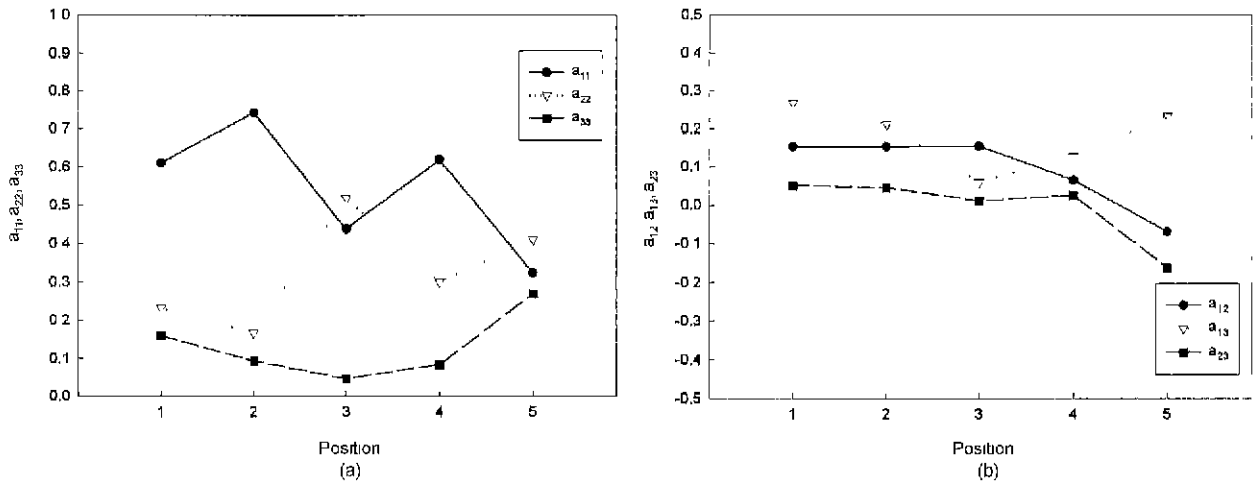

Figure 10. Components of the orientation tensor along the location '**e**' defined in Figure 5 at different positions: (a) diagonal components, (b) off-diagonal components.

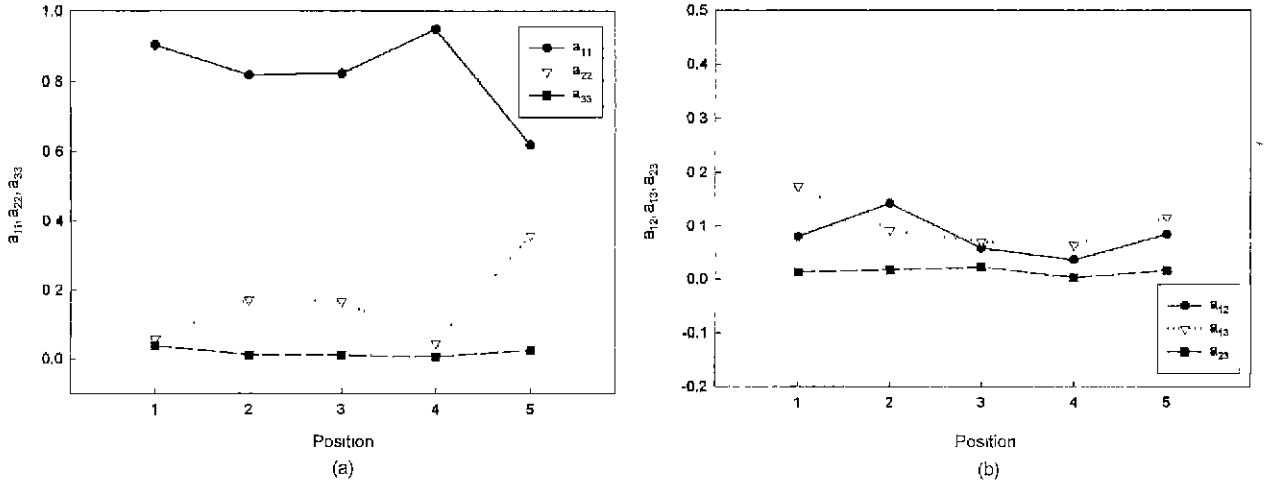

Figure 11. Components of the orientation tensor along the location '**f**' defined in Figure 5 at different positions: (a) diagonal components, (b) off-diagonal components.

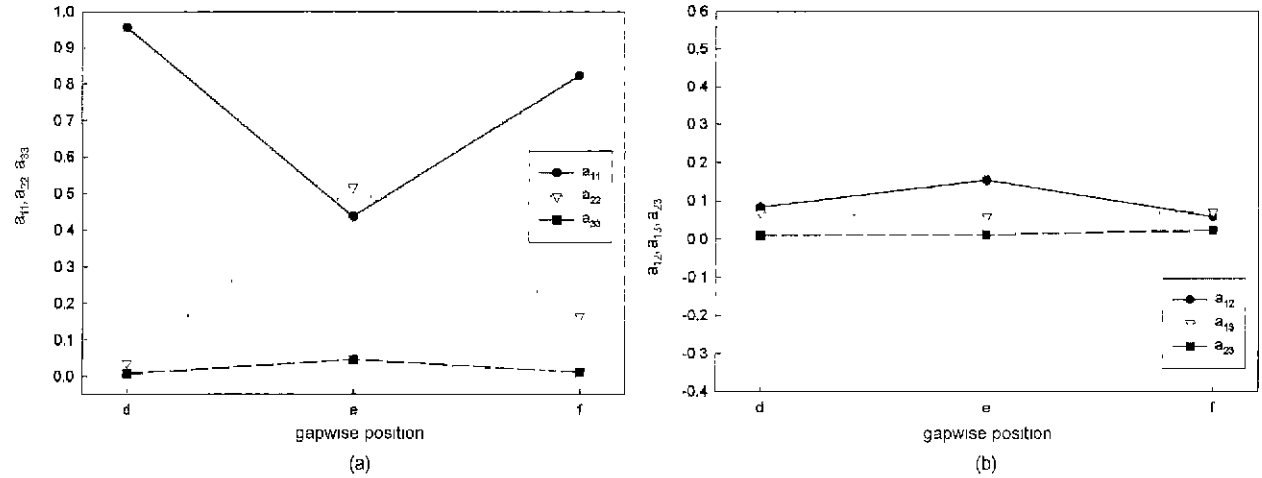

Figure 12. Components of the orientation tensor with respect to the thickness at the center of position 3: (a) diagonal components, (b) off-diagonal components.

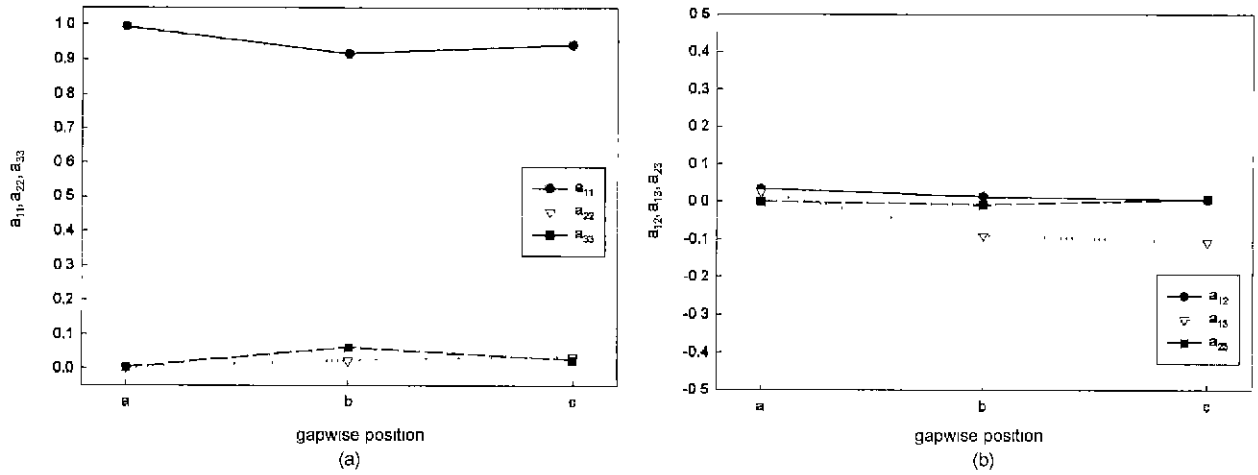

Figure 13. Components of the orientation tensor with respect to the thickness at the edge of position 4: (a) diagonal components, (b) off-diagonal components.

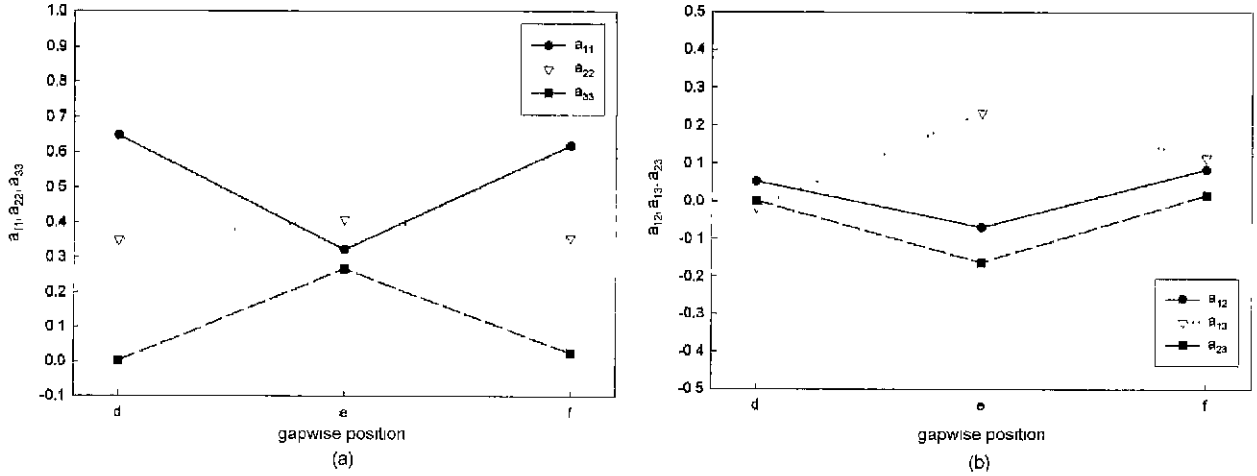

Figure 14. Components of the orientation tensor with respect to the thickness at the center of position 5: (a) diagonal components, (b) off-diagonal components.

those at the positions 1, 2, and 5, the fibers at the position 3 are distributed randomly in a plane. Fibers are randomly oriented three dimensionally at the position 5 ($a_{11} = 0.32$, $a_{22} = 0.41$, and $a_{33} = 0.27$). In Figure 11, a_{33}, a_{13}, and a_{23} have small values along the point 'f' so that the orientation is almost planar. At the converging region (position 2), fibers are slightly rotated from the x-direction to the y-direction. Along to point 'f', fibers are highly aligned to the flow direction at the position 3 and are rather randomly oriented at the end of specimen.

Orientation states with respect to the thickness

A shell-core structure[22,23] appears at the center of the position 3 in Figure 12. Since the orientation of fibers near the wall are affected by strong shear flow most fibers are aligned along the flow direction. On the other hand, fibers near the core are randomly oriented because shear deformation rates are reduced and some elongational effects are present. As shown in Figure 13, there is also strong shear effect at the edge and the shell-core structure does not appear. Figure 14 shows that the fibers are partially oriented in the x-direction and in the y-direction both in upper and in lower shells. In the core, almost three-dimensional random orientation state is shown. It is believed that the fountain flow in the melt front region during filling causes the fibers to be oriented randomly.

Visual representation of orientation states

The eigenvectors of the orientation tensor can represent three-dimensional orientation states[24] as shown in Figure 15. The eigenvectors of the second order orientation tensor denote principal directions of orientation and corresponding

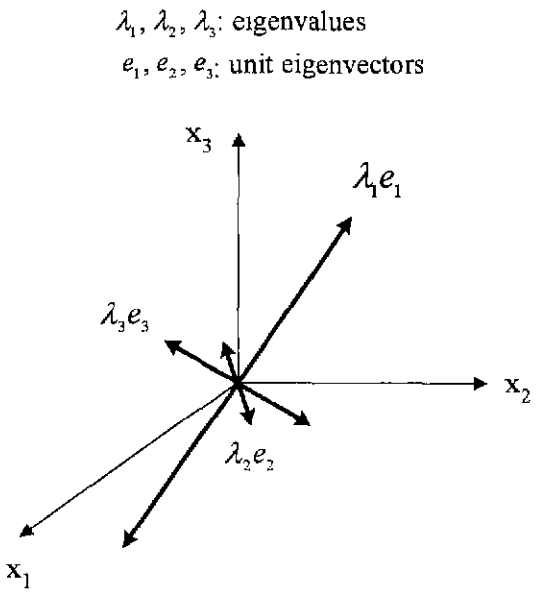

Figure 15. Principal directions of orientation defined by second order orientation tensor.

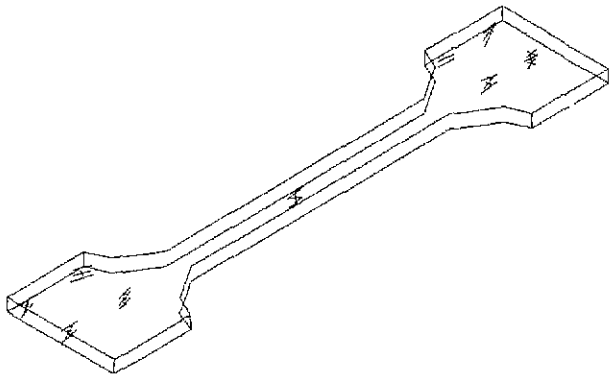

Figure 16. Three-dimensional representation of the principal directions of orientation tensors.

eigenvalues indicate degree of orientation in their principal directions. Therefore the projections of the eigenvectors on any surface can be used to describe the orientation state in that plane.

Figures 16 to 18 show the visual representation of three-dimensional orientation state by using eigenvectors and eigenvalues. Each line represents eigenvector of the orientation tensor and the length of each line equals magnitude of the corresponding eigenvalue. Here, the length of each line is taken to be twice the eigenvalue for good visualization. Overall orientation states of the specimen are shown in Figure 16. The principal directions of orientation tensors projected onto the x-y plane are described in Figure 17 and those projected onto the y-z plane are shown in Figure 18.

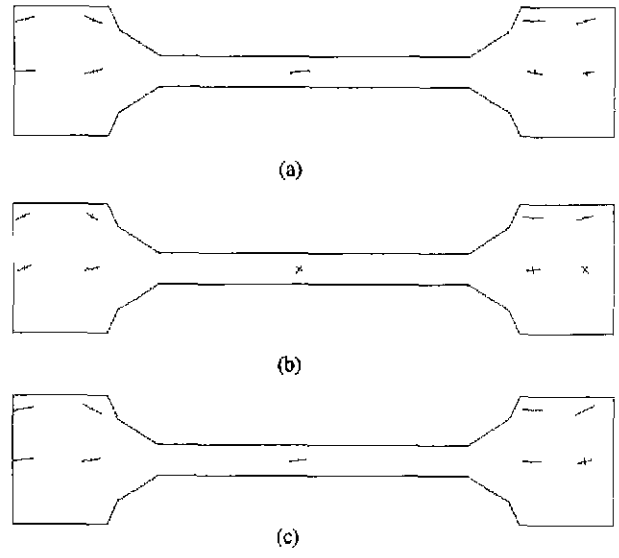

Figure 17. Principal directions of orientation tensors projected onto the x-y plane: (a) upper-plane, (b) mid-plane, (c) lower-plane.

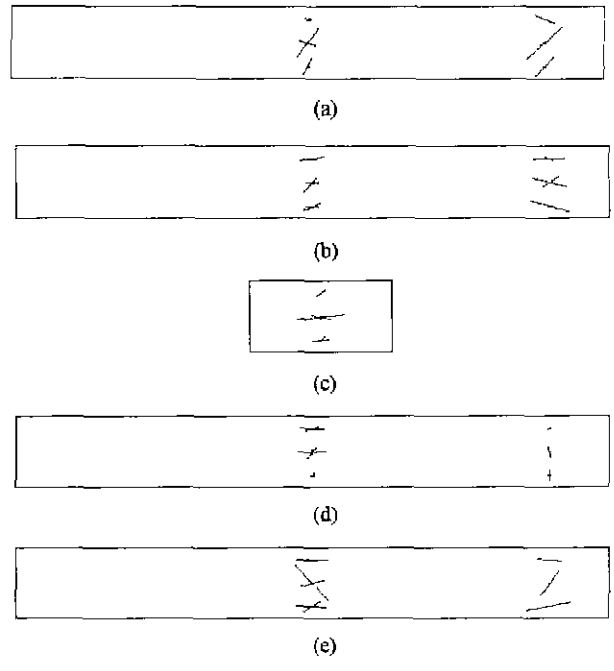

Figure 18. Principal directions of orientation tensors projected onto the y-z plane. (a) position 1, (b) position 2, (c) position 3, (d) position 4, (e) position 5.

Conclusions

The use of CLSM makes it possible to remove the ambiguity in determining the off-diagonal components of orientation tensors and to measure three-dimensional fiber orientation states in SFRP. The second order orientation

tensor is used for describing the orientation state. The orientation tensors are obtained at different positions along the flow direction as well as in the thickness plane of the specimen. In general, the specimen has the shell-core structure, where fibers are highly aligned to the flow direction near the mold-wall and randomly oriented in the core of the specimen. In the middle of the specimen the layered shell-core structure has developed. At the edge of diverging region fibers are fully aligned to the flow direction across the thickness. Near the gate, out-of-plane orientation components are not negligible in the core or in the lower shell. From near the gate to the converging region, fibers are rotated from one direction to the other at the edge. At the end of the cavity, planar random orientation states appear in the upper and lower shells and three-dimensional random orientation state is developed in the core.

Acknowledgements

This study was supported by research grants from the Ministry of Science and Technology through the National Research Lab (NRL). The authors are grateful for the support.

References

1. J. Ko and J. R. Youn, *Polym. Compos.*, **16**, 114 (1995).
2. S. C. Lee, D. Y. Yang, J. Ko, and J. R. Youn, *J. Mat. Proc. Tech.*, **70**, 83 (1997).
3. S. W. Lee and J. R. Youn, *Macromolecular Sympo.*, **148**, 263 (1999).
4. K. H. Lee and J. R. Youn, *Polym. Compos.*, **13**, 251 (1992).
5. H. H. Shim, O. K. Kwon, and J. R. Youn, *Wear*, **157**, 141 (1992).
6. H. H. Shim, O. K. Kwon, and J. R. Youn, *Polym. Compos.*, **11**, 337 (1990).
7. S. W. Yurgartis, *Comp. Sci. Tech.*, **30**, 279 (1987).
8. P. J. Hine, N. Davidson, R. A. Duckett, A. R. Clarke, and I. M. Ward, *Polym. Compos.*, **17**, 720 (1996).
9. L. Avérous, J. C. Quantin, A. Crespy, and D. Lafon, *Polym. Eng. Sci.*, **37**, 329 (1997).
10. J. J. McGrath and J. M. Wille, *Comp. Sci. Tech.*, **53**, 133 (1995).
11. J. L. Thomason and A. Knoester, *J Mater. Sci. Lett.*, **9**, 258 (1990).
12 S. H. McGee and R. L. McCullough, *J. Appl Phys.*, **55**, 1394 (1984).
13. S. G. Advani and C. L. Tucker III, *J. Rheol.*, **31**, 751 (1987).
14. R. S. Bay and C. L. Tucker III, *Polym. Eng. Sci.*, **32**, 240 (1992).
15. A. R. Clarke, G. Archenhold, and N. C. Davidson, *Comp Sci. Tech.*, **55**, 75 (1995).
16. A. R. Clarke, G. Archenhold, and N. C. Davidson in "Microstructural characterisation of fibre-reinforced composites", (J. Summerscales Ed.), pp.55-137, Woodhead publishing limited, Cambridge, 1998.
17. L. C. Sawyer and D. T. Grubb, "Polymer Microscopy", Chapman and Hall, London, 1989.
18. Y. H. Lee, MS thesis, Seoul National University, Seoul, 1999.
19. A. K. Jain, "Fundamentals of digital image processing", Prentice Hall, Englewood Cliffs, 1989.
20. H. Yang and J. S. Colton, *Polym. Compos.*, **15**, 46 (1994).
21. C. L. Tucker III and S. G. Advani in "Flow and rheology in polymer composites manufacturing", (S. G Advani Ed.), pp.147-202, Elsevier, Amsterdam, 1994.
22. R. S. Bay and C. L. Tucker III, *Polym. Compos.*, **13**, 317 (1992).
23. R. S. Bay and C. L. Tucker III, *Polym. Compos.*, **13**, 332 (1992).
24. M. C. Altan, S. Subbiah, S. I. Güçeri, and R. B. Pipes, *Polym. Eng. Sci.*, **30**, 848 (1990).